

Cross-polarization gain calibration of linearly polarized VLBI antennas by observations of 4C 39.25

F. Jaron^{1,2}, I. Martí-Vidal^{3,4}, M. Schartner⁵, J. González-García⁶,
E. Albentosa-Ruiz⁴, S. Bernhart^{7,8,2}, J. Böhm¹, J. Gruber¹, S. Modiri⁸,
A. Nothnagel¹, V. Pérez-Díez^{9,6}, T. Savolainen^{10,11,2}, B. Soja⁵, E. Varenius¹²,
M. H. Xu^{13,10}

¹ Technische Universität Wien, Wiedner Hauptstraße 8-10, 1040 Wien, Austria

² Max-Planck-Institut für Radioastronomie, Auf dem Hügel 69, 53121 Bonn, Germany

³ Departament d'Astronomia i Astrofísica, Universitat de València, C. Dr. Moliner 50, 46100, Burjassot, València, Spain

⁴ Observatori Astronòmic, Universitat de València, Parc Científic, C. Catedràtic José Beltrán 2, 46980, Paterna, València, Spain

⁵ Institute of Geodesy and Photogrammetry, ETH Zürich, 8093 Zürich, Switzerland

⁶ Centro Astronómico de Yebes (IGN), Apartado 148, 19180, Yebes, Spain

⁷ Reichert GmbH, 53129 Bonn, Germany

⁸ Federal Agency for Cartography and Geodesy (BKG), Department Geodesy, Frankfurt am Main, Germany

⁹ Observatorio Astronómico Nacional (OAN-IGN), Alfonso XII 3, 28014 Madrid, Spain

¹⁰ Aalto University Metsähovi Radio Observatory, Metsähovintie 114, 02540 Kylmälä, Finland

¹¹ Aalto University Department of Electronics and Nanoengineering, PO Box 15500, 00076 Aalto, Finland

¹² Chalmers University of Technology, Gothenburg, Sweden

¹³ GFZ German Research Centre for Geosciences, 14473 Potsdam, Germany

Key Points:

- The new-generation geodetic radio telescopes observe two orthogonal linear polarization directions.
- Calibration of the gain differences between the two polarizers is necessary to maximize the signal-to-noise ratio of observations.
- We investigate these cross-polarization gain differences and their temporal evolution for selected antennas.

Corresponding author: Frédéric Jaron, frederic.jaron@tuwien.ac.at

Abstract

Radio telescopes with dual linearly polarized feeds regularly participate in Very Long Baseline Interferometry (VLBI). One example is the VLBI Global Observing System (VGOS), which is employed for high-precision geodesy and astrometry. In order to achieve the maximum signal-to-noise ratio, the visibilities of all four polarization products are combined to Stokes I before fringe-fitting. Our aim is to improve cross-polarization bandpass calibration, which is an essential processing step in this context. Here we investigate the shapes of these station-specific quantities as a function of frequency and time. We observed the extra-galactic source 4C 39.25 for six hours with a VGOS network. We correlated the data with the DiFX software and analyzed the visibilities with PolConvert to determine the complex cross-bandpasses with high accuracy. Their frequency-dependent shape is to first order characterized by a group delay between the two orthogonal polarizations, in the order of several hundred picoseconds. We find that this group delay shows systematic variability in the range of a few picoseconds, but can remain stable within this range for several years, as evident from earlier sessions. On top of the linear phase-frequency relationship there are systematic deviations of several tens of degrees, which in addition are subject to smooth temporal evolution. The antenna cross-bandpasses are variable on time scales of ~ 1 hour, which defines the frequency of necessary calibrator scans. The source 4C 39.25 is confirmed as an excellent cross-bandpass calibrator. Dedicated surveys are highly encouraged to search for more calibrators of similar quality.

1 Introduction

Antennas participating in Very Long Baseline Interferometry (VLBI) have traditionally been observing with circularly polarized feeds (Thompson et al., 2017). New developments make it necessary that antennas also observe in linear polarization. One such example, and the subject of this paper, is the VLBI Global Observing System (VGOS, Petrachenko et al., 2009, still under the name of “VLBI2010”). Aimed at improving the precision of geodetic and astrometric VLBI (Sovers et al., 1998) down to mm and sub-mm/year scales, it was recognized that this requires an extension of the observed bandwidth to the range of 2 to 15 GHz. Such a bandwidth is best realized with the use of linear feeds, because $\lambda/4$ -plates, necessary for the realization of circular polarization, do not work over such a large frequency range. See, however, Abdalmalak et al. (2020) for the possibility of using circularly polarized log-spiral antennas for reception and Jaradat et al. (2021) for emission of broadband radio signals.

Using linear feeds requires that the telescopes simultaneously observe two perpendicular polarization directions. Throughout this paper, we are going to refer to these polarization directions as “H” for horizontal and “V” for vertical. In the context of VGOS, these polarization directions are also referred to as “X” and “Y”. However, this terminology is invalid because the linear feeds of VGOS antennas are not aligned with celestial coordinate axes. Two polarization directions are necessary because non-zero parallactic angle differences between the telescopes of long baselines generally cause a loss of signal-to-noise ratio (SNR) of the parallel hand polarization products. In order to obtain the full SNR for all parallactic angles it is necessary to combine all four polarization products with each other to form Stokes I for fringe-fitting. The formula for Stokes I_{ab} for a baseline consisting of telescopes a and b is

$$I_{ab} = (H_a H_b + \rho_a \rho_b^* V_a V_b) \cos \Delta + (\rho_b^* H_a V_b - \rho_a V_a H_b) \sin \Delta, \quad (1)$$

where the terms $H_a H_b$ and $V_a V_b$ are the “parallel-hand” linear polarization correlation products (i.e., visibilities), and $H_a V_b$ and $V_a H_b$ and the “cross-hand” products. The coefficients $\rho_{a,b}$ denote the complex gain differences between the H and V polarizers at each antenna a and b, in terms of amplitude A and phase φ , i.e., $\rho = Ae^{i\varphi}$. Finally, Δ is the parallactic angle difference between the antennas a and b. Obviously, for the realization

81 of coherent summation of the correlator visibilities, the computation of Stokes I requires
 82 information about the complex gain differences ρ between the two linear feeds of each
 83 antenna participating in the observation. We will refer to this quantity, which is a func-
 84 tion of frequency over the observed bandwidth, as the *cross-polarization bandpass* (or
 85 simply *cross-bandpass*). The investigation of the cross-bandpasses, both as a function
 86 of frequency and time, i.e., $\rho(\nu, t)$, is the subject of this article. Equation (1) makes it
 87 evident that well-determined cross-polarization bandpasses are a key quantity for any
 88 VLBI experiments in which linearly polarized antennas participate.

89 Cross-bandpass calibration is a processing step that is commonly carried out for
 90 each VGOS session after correlation and before final fringe-fitting. The approach that
 91 is currently being applied is to use observations of the session to be processed also for
 92 the determination of the cross-bandpasses. One procedure, developed at MIT Haystack
 93 Observatory, applying the program `fourfit`, is described in Niell et al. (2018), and has
 94 become the generally adopted method for the processing of VGOS experiments (A de-
 95 tailed description of the procedure can be found in this document: [https://www.haystack](https://www.haystack.mit.edu/wp-content/uploads/2020/07/docs_hops_000_vgos-data-processing.pdf)
 96 [.mit.edu/wp-content/uploads/2020/07/docs_hops_000_vgos-data-processing.pdf](https://www.haystack.mit.edu/wp-content/uploads/2020/07/docs_hops_000_vgos-data-processing.pdf),
 97 accessed on October 2, 2023, as all other links in this article). However, the software `PolConvert`
 98 (Martí-Vidal et al., 2016) offers an alternative route for VGOS data processing. For the
 99 investigations at hand, we make use of the capability of `PolConvert` to estimate the cross-
 100 polarization gains with configurable spectral resolution and time averaging.

101 The principal functionality of `PolConvert` is to convert visibilities of linearly po-
 102 larized data to a circularly polarized basis. For optimal results, cross-polarization band-
 103 pass calibration is an essential processing step. Compared to the cross-bandpass calibra-
 104 tion implemented in the Haystack Observatory Postprocessing System (HOPS), the al-
 105 gorithm in `PolConvert` is potentially superior, because it makes use of both amplitude
 106 and phase of the visibilities, and also offers the possibility to use the instrumental phase-
 107 calibration signal (“phase-cal”) to determine delays between H and V polarization. The
 108 code performs a least-squares fitting of the visibility data directly without fringe-fitting.
 109 `PolConvert` has been used to convert ALMA observations from linear to circular for the
 110 Event Horizon Telescope (Event Horizon Telescope Collaboration et al., 2019) and also
 111 for the Global mm-VLBI Array (Zhao et al., 2022). However, in both of these cases, the
 112 cross-bandpasses were calibrated using pre-determined calibration tables. The applica-
 113 bility of `PolConvert` to VGOS data has been demonstrated by Alef, Tuccari, et al. (2019)
 114 and further described by Martí-Vidal et al. (2021), in which case the cross-bandpasses
 115 are determined from calibration scans. The different processing steps of `PolConvert` can
 116 be run separately. Here we make use of the step that determines the cross-polarization
 117 gains as a tool to estimate these quantities for the analysis presented in this article.

118 Because cross-polarization bandpass calibration is a crucial step in the VGOS pro-
 119 cessing chain, the aim of our investigation is to measure and characterize the cross-bandpasses
 120 of VGOS antennas. For an optimal measurement, two requirements are of essential im-
 121 portance. First, the observed radio source has to be a suitable calibrator. Prior to our
 122 investigations presented here, we examined a number of calibrator scans that were ob-
 123 served as part of research and development (R&D) sessions of the EU-VGOS project (Alef,
 124 Anderson, et al., 2019a; Jaron et al., 2021; Albentosa et al., 2023). An inspection of the
 125 cross-bandpass solutions from multiple calibrator scans has revealed that there are huge
 126 differences in their quality and that there is an obvious dependency on the observed source.
 127 There is one source for which the results stand out compared to other sources, and this
 128 is the radio-loud active galactic nucleus (AGN) 4C 39.25. Secondly, the observing geom-
 129 etry is critical, in particular the coverage of the parallactic angle. For the research pre-
 130 sented here, we designed a session that uses this knowledge for the optimal measurement
 131 of the cross-bandpasses of the VGOS antennas that participated in our observations.

132 Another possibility of realizing dual circular polarization for broadband receivers,
 133 such as VGOS, is the use of so-called 3dB/90° microwave hybrid couplers. These devices

offer a hardware solution to convert dual linear into dual circular polarization, and can be installed at the telescopes before the low-noise amplifiers. Their potential suitability for VGOS has been described in a technical report (García-Pérez, Terceroc, Malo, & López-Pérez, 2018). In another technical report García-Pérez, Terceroc, Malo, Gallego, and López-Pérez (2018) discuss these devices as a possibility for the BRAND receiver (Alef, Anderson, et al., 2019b). In the time of writing, the only VGOS observing mode that has so far been carried out is to record the data in linear polarization and account for this during the digital data processing after correlation, and we are going to assume this mode in the remainder of this article. It is important to note that also in the case that the data are recorded in dual circular polarization, if ones wants to combine the data to Stokes I , it is still necessary to determine the cross-polarization bandpass (between R and L) and to properly calibrate the data. Also, an additional device, such as a hybrid coupler, comes at the risk of introducing additional systematic errors (as discussed in the two technical reports mentioned) and degrading the signal-to-noise ratio. For these reasons, we tentatively conclude that for broadband observations the use of dual linear polarization along with a software solution is the better option. However, we strongly encourage experiments to test observing with hybrid couplers. More information about hybrid couplers can be found in a number of publications (Malo-Gomez et al., 2009; Khudchenko et al., 2019; López-Pérez et al., 2021; Kooi et al., 2023).

The paper is organized as follows. We give a brief introduction to the astrophysical object 4C 39.25 in Sect. 2. In Sect. 3 we describe the properties of our VGOS R&D session. We describe our methods in Sect. 4 and present our results in Sect. 5. We give our conclusions in Sect. 6.

2 The source 4C 39.25

During the inspection of the results of cross-bandpass calibration from different scans that were initially scheduled for this purpose in previous sessions, it turned out that the quality of the results was variable and that there was an apparent dependency on the radio source under observation. Among the many sources that were each observed multiple times with 2-3 minute scans, one source always stood out in terms of cleanliness of the cross-bandpass solution, and that was 4C 39.25. For this reason, we have chosen this source as the target for our dedicated experiment with the aim of measuring and investigating the cross-bandpasses of VGOS antennas.

Discovered during a survey of radio sources (Pilkington & Scott, 1965), 4C 39.25 (B1950 name 0923+392) soon became a target of astrophysical interest. Linear polarization of its radio emission was detected (Berge & Seielstad, 1969; Aller, 1970), and Bignell and Seaquist (1973) even published a time-series of polarization. Nartallo et al. (1998) classify the source as a “low polarization quasar” (see their Table 2), referring to the research by Impey and Tapia (1990). Indeed, Impey and Tapia (1990) report a polarization of $p = 0.5 \pm 0.5$, which indicates that p is equal to zero, i.e., that the source is not polarized. However, this value has been derived for the optical emission from this source (see their Table 1). In the same article, the authors also come to the conclusion that optical and radio polarization are not correlated, which in turn means that it cannot be ruled out that the radio emission from 4C 39.25 could still be polarized to some degree. Alberdi et al. (2000) present VLBI observations at 15, 22, and 43 GHz, showing that features in the jet are polarized while the component that they interpret as the core is not polarized at radio wavelengths. In addition to that, Alberdi et al. (2000) report some features in the jet to move at apparently superluminal speeds, implying that Doppler boosting of the intrinsic emission plays an important role for this source. The source is also in the MOJAVE Survey (see <https://www.cv.nrao.edu/MOJAVE/sourcepages/0923+392.shtml>).

Table 1. List of stations included in the schedule for the session er2201.

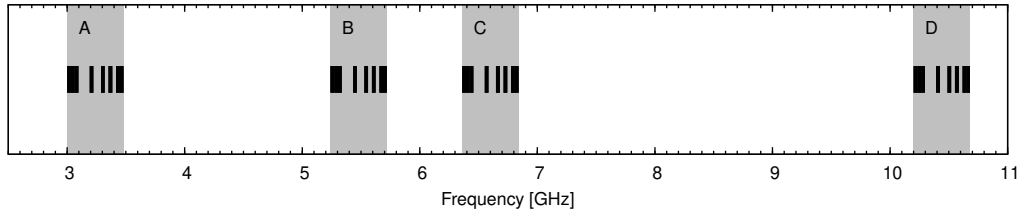
Code	Name	Description	Comment
Mg	MACGO12M	McDonald Geodetic Observatory (MGO), TX, USA	1
Oe	ONSA13NE	Onsala 13-m antenna north-east, Sweden	
Ow	ONSA13SW	Onsala 13-m antenna south-west, Sweden	
Wf	WESTFORD	Westford, MA, USA	
Ws	WETTZ13S	Wettzell 13-m antenna south, Germany	
Yj	RAEGYEB	13-m at Yebes, Spain	2

¹ For Mg, data only partly available after 2 hours.

² Yj did not observe VGOS band D.

Table 2. Frequency setup. The four VGOS bands are labeled A-D, each has a bandwidth of 480 MHz with a frequency range as given in the table. Each band is further divided into eight IF sub-bands with a bandwidth of 32 MHz each, the upper bounds of which are given in the table.

Band	Min. freq.	IF upper bounds [MHz]							
A	3000.4	3032.4	3064.4	3096.4	3224.4	3320.4	3384.4	3448.4	3480.4
B	5240.4	5272.4	5304.4	5336.4	5464.4	5560.4	5624.4	5688.4	5720.4
C	6360.4	6392.4	6424.4	6456.4	6584.4	6680.4	6744.4	6808.4	6840.4
D	10200.4	10232.4	10264.4	10296.4	10424.4	10520.4	10584.4	10648.4	10680.4

**Figure 1.** Frequency setup of our observations. The letters A, B, C, and D refer to the VGOS band labels. See Table 2 for details.

3 The VLBI session er2201

For the purpose of measuring the cross-bandpasses of VGOS antennas, we carried out a dedicated R&D session. The principal idea was to observe 4C 39.25, which we had identified as an excellent cross-bandpass calibrator, for six hours. Here we describe the details of this session, which was carried out under the name “er2201”.

3.1 Scheduling

The scheduling for the session er2201 was performed with the software VieSched++ (Schartner & Böhm, 2019). The session was observed on September 8, 2022, from 11:30 to 17:30 UTC. The network consisted of the VGOS stations Mg, Oe, Ow, Wf, Ws, and Yj. Details about the stations are given in Table 1.

The frequency setup of our observation is identical to the one currently used for global VGOS sessions (Niell et al., 2018) and is listed in Table 2. We follow the convention of the VGOS community and label the four bands with letters A, B, C, D. Each of these bands has a frequency range of 480 MHz and is further divided into eight sub-bands

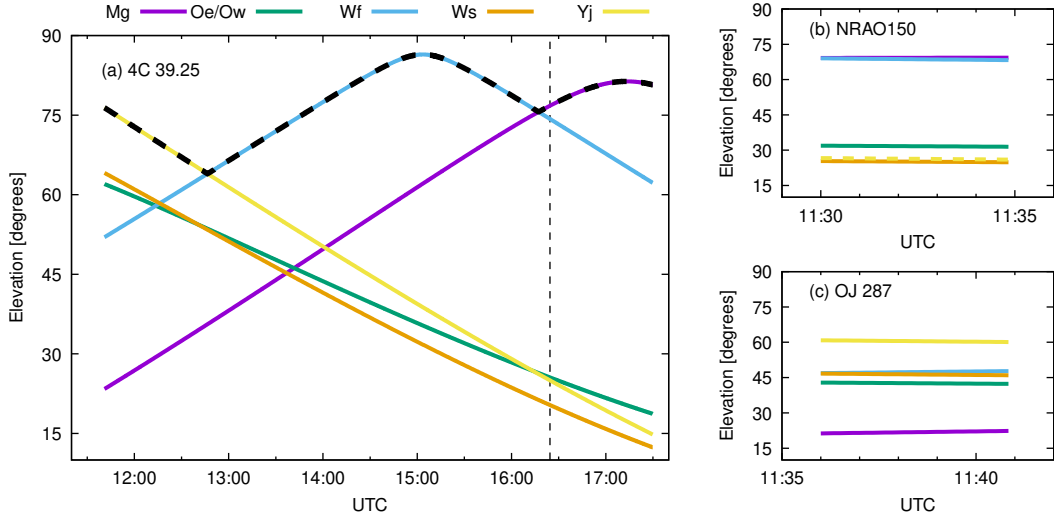


Figure 2. Antenna elevations as a function of time for day 2022-09-08. (a) Observations of 4C 39.25. The position of scan 143 (reference scan) is marked by the dashed vertical line at 16:24 UTC. The dashed curves highlight the upper envelope of elevations. (b) Elevations for the observation of NRAO150. Station Yj missed this scan as indicated by the dash line. (c) Elevations for the observation of OJ287.

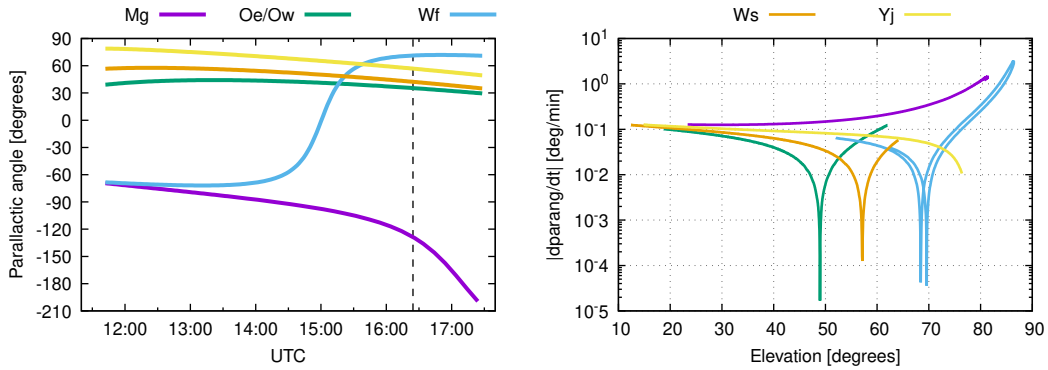


Figure 3. Left: Parallax angle against observation time. Right: Absolute value of the time derivative of the parallax angle, plotted against elevation angle.

198 of 32 MHz bandwidth each. All of these sub-bands are realized as lower side-bands, which
 199 is why the upper bounds of these bands are given in Table 2. A visualization of the frequ-
 200 eency setup can be seen in Fig. 1. The frequency spans of the four VGOS bands
 201 are presented by the grey-shaded areas, and the distributions of the sub-bands within these
 202 bands are shown as black areas.

203 The session started with two 5-min scans of the two radio-loud AGNs NRAO150
 204 and OJ287. These scans were included in the schedule with the aim of investigating the
 205 potential suitability of other sources as cross-bandpass calibrators. These two sources
 206 were chosen because they were also giving good results in the past, albeit not as good
 207 as 4C 39.25. The remainder of the session consists of a series of repeated 10-min scans
 208 on 4C 39.25. In order to give the electronics at the stations the time to reset, gaps of du-
 209 ration 5 seconds were scheduled in between scans.

210 Cross-polarization bandpass calibration requires a large enough parallactic angle
 211 coverage. In principle, it is possible to determine the amplitudes and phases of the cross-
 212 gains within a few minutes of observation if the parallactic angle of one antenna changes
 213 fast enough. In practice this means that it is sufficient that one antenna of the network
 214 of a scan observes the source with a large elevation angle; ideally, the source would be
 215 observed *in transit*. Our scheduling approach was thus to search for a 6-hours time win-
 216 dows, within the 24 hours of a day, during which a network of VGOS telescopes could ob-
 217 serve our target source 4C 39.25 such that one antenna in each scan always has a large
 218 elevation angle. In Fig. 2, panels (a) to (c) show the elevation angle of each antenna as
 219 a function of time. The plot in panel (a) refers to observations of the main target 4C 39.25.
 220 The elevation angle of the two other candidate sources, observed in the beginning of the
 221 session, are plotted in the two panels of the right-hand side, observations of NRAO 150
 222 in panel (b) and OJ 287 in panel (c).

223 The fact that a high elevation angle of one participating antenna is crucial for the
 224 quality of the cross-bandpass solution means that an important quantity is the upper
 225 envelope of the elevation plot shown in Fig. 2 (a). This upper envelope is plotted as the
 226 black dashed line. It is made up of the curves for station Yj from the beginning until $\sim 12:45$.
 227 After that Wf takes over and has the highest elevation of the network until about 16:15,
 228 when this role is given to station Mg until the end of the session. The importance of these
 229 stations during these observational time spans should be kept in mind in the context of
 230 data issues, as explained further down in the text.

231 How large should the elevation angle of an antenna be to guarantee a large enough
 232 parallactic angle coverage? The left-hand panel of Fig. 3 shows the parallactic angle of
 233 each antenna as a function of observation time. Color coding, time range, and source are
 234 the same as in Fig. 2, allowing a direct comparison of the two figures. Indeed, there is
 235 a correspondence of steep slopes of the parallactic angles in left-hand panel of Fig. 3 dur-
 236 ing times of high elevations in Fig. 2 (a). This is particularly evident for station Wf, which
 237 has an elevation of almost 90° at around 15:00 UTC, resulting in a very high slope of par-
 238 allactic angle during the same time. A similar correspondence can be seen for station
 239 Mg around 17:00 UTC. To investigate the dependency between elevation and parallac-
 240 tic angle coverage in more detail, the right-hand panel of Fig. 3 presents the absolute value
 241 of the time derivative of the parallactic angle, plotted against the elevation angle for each
 242 antenna. The y -axis has a logarithmic scale and is given in units of degrees per minute.
 243 And indeed, parallactic angle rates of several degrees per minute are reached for eleva-
 244 tion angles above $\sim 80^\circ$ for station Mg and for elevation angles above $\sim 85^\circ$ for sta-
 245 tion Wf. However, the elevation dependency is not so simple in the sense that a larger
 246 elevation angle automatically means a larger parallactic angle coverage. Based on this
 247 plot, an elevation angle larger than approximately $80^\circ - 85^\circ$ should guarantee a par-
 248 allactic angle coverage of several degrees in a single scan with a duration of a few min-
 249 utes, which is enough to break the degeneracy in the system of equations to compute the
 250 complex cross-polarization bandpass.

251 3.2 The data

252 Figure 4 presents a plot showing the observing times of each station that partic-
 253 ipated in er2201. As indicated by the line colors, two candidate sources were observed
 254 at the beginning of the session: NRAO150 (purple) and OJ 287 (green). For the remain-
 255 der of the session, the source 4C 39.25 (black) was observed exclusively.

256 Two stations had issues during the session. Yj missed the first scan to the source
 257 NRAO150, and throughout the entire session, this station did not record the VGOS band D.
 258 This fact is indicated by the line width, which is thinner for this station than for the other
 259 stations. Station Yj is responsible for the highest elevation angles in the beginning of
 260 the session until about 12:45, which should be kept in mind when interpreting results.

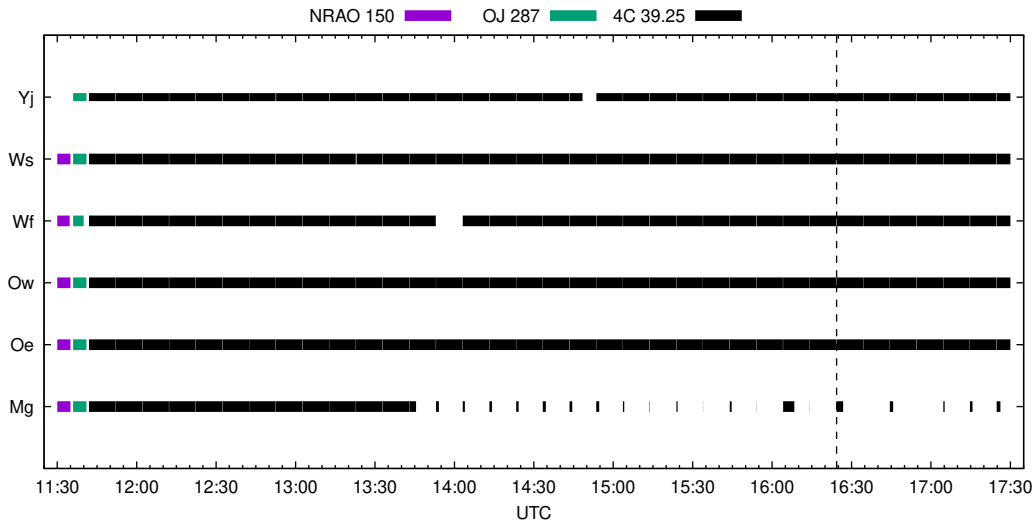


Figure 4. Observation times and data availability of the participating stations. The session er2201 lasted from 11:30 until 17:30 UTC on September 8, 2022. For station Mg data from 13:43 on are only partly available. The line for station Yj appears thinner than the lines for the other stations to indicate that Yj did not record the full bandwidth, missing VGOS band D. The vertical dashed line marks the position of scan 143, which serves as the reference scan.

261 The other major issue occurred at station Mg. For the first two hours of the ses-
 262 sion, the data from this station are fully available. But then starting at 13:43 UTC only
 263 fractions of the scheduled scan lengths are available. This fact corresponds to the spar-
 264 sity of the line in Fig. 4 for that station from that moment on. The reason for this data
 265 loss has been identified to be a software issue used in combining the data that has been
 266 fixed (Chet Ruszczyk, MIT Haystack Observatory, priv. comm.). There is, however, un-
 267 fortunately no way to recover these data anymore for the original data was deleted. The
 268 missing data for Mg, especially during the later times of this session, is a matter of con-
 269 cern because Mg marks the upper envelope of the elevation plot from about 16:15 on (see
 270 the dashed line in Fig. 2 a).

271 Besides these two major issues, only two gaps appear in the data for Yj ($\sim 14:40$,
 272 where only data for VGOS band A are missing) and Wf ($\sim 14:00$, all bands missing).
 273 Otherwise we have a solid database to analyze from this session.

274 4 Methods

275 The data processing for our present work consists of correlation of the raw obser-
 276 vational data and analysis of the resulting visibilities with the software `PolConvert`. Here
 277 we describe our methods.

278 4.1 Correlation

279 The data were correlated at the VLBI correlator of the Technical University of Vi-
 280 enna (TU Wien), making use of the Vienna Scientific Cluster (VSC4, <https://vsc.ac.at/systems/vsc-4/>). We used the DiFX software correlator (Deller et al., 2011) in its
 281 version 2.5.4, which is the current version to be used for the correlation of VGOS data
 282 (Jaron et al., 2021). For the analysis of the present work, we divided the original 10-min
 283 scans into slices of 2-min by editing the vex control file. We then correlated the data with
 284

Table 3. PolConvert processing steps.

	Description
0	Source scanner (Initial fringe-fitting, SNR estimate)
1	Estimate cross-polarization gains
2	PolConvert the whole experiment
3	Estimate additive phases and write fourfit control file
4	Calibrate bandpass and remove IONEX TEC (optional)
5	Perform broadband Global Fringe Fitting (optional)
6	Write fully calibrated SWIN files

285 a spectral resolution of 250 kHz (i.e., 128 channels per sub-band of bandwidth 32 MHz)
 286 with a length of the accumulation periods of 1 second.

287 4.2 Cross-polarization bandpass calibration

288 We use the PolConvert software (Martí-Vidal et al., 2016, 2021) for the determi-
 289 nation of the cross-bandpasses. In its current version, PolConvert distinguishes seven
 290 processing steps (numbered 0 to 6), as listed in Table 3. These steps can be run indi-
 291 vidually.

292 Step number 0 (“Source scanner”) carries out an initial fringe-fitting of each scan
 293 in order to estimate the signal-to-noise ratio (SNR). In the masterfile (a Python script
 294 that serves as the user interface to PolConvert) one can configure the sub-bands to be
 295 included in the fringe-fitting. For our present analysis, we include all 32 sub-bands. In
 296 the output file of step 0, PolConvert reports the information on whether a scan is suit-
 297 able for the estimation of the cross-gains along with detailed information about the SNR
 298 of each antenna and sub-band.

299 In step 1 the cross-polarization bandpasses are estimated as a complex quantity,
 300 i.e., the complex gain differences between the two polarizers as a function of frequency
 301 for each antenna. The user has the possibility to configure how many spectral channels
 302 the algorithm averages and the integration time. For the data of our experiment, it turns
 303 out that averaging over eight channels and an integration time of 20 seconds gives the
 304 best results. We use PolConvert step 1 with this configuration for the estimation of the
 305 cross-polarization bandpasses presented further down in this article. For this step, and
 306 for all of the subsequent analyses, we exclude the very short baseline between the On-
 307 sala twin telescopes. The reason for this is that, because of the constantly very low fringe
 308 rate on this baseline, the phase-cal signal always interferes and dominates the cross-power
 309 spectrum. Flagging of the affected channels would be another means of mitigating this
 310 problem, but we choose to eliminate this baseline altogether in order to avoid any con-
 311 tamination at all.

312 Step 2 converts the visibilities for the entire experiment from linear to circular po-
 313 larization. It uses the results from step 1 for the calibration of the complex cross-polarization
 314 gain differences between the two linear feeds of each antenna.

315 Residual phase-offsets between sub-bands are corrected for in PolConvert step 3,
 316 which writes a Fourfit control file containing the corresponding phase corrections. It
 317 can be used for the final fringe-fitting of the data with the HOPS Fourfit program.

318 The last three steps are not used for the analysis presented in this article. We are
 319 just listing them here for completeness.

5 Results

Here we present the results from our analysis of the visibilities to estimate the cross-polarization bandpasses of the participating stations, using the software `PolConvert` (Martí-Vidal et al., 2016), as described in the previous section. First, we investigate the dependency of amplitude and phase of the cross-bandpasses as a function of frequency (Sect. 5.1), then we explore their evolution with time (Sect. 5.2).

An eye-inspection of the results for the 175 2-minute scans made it evident that, while most of the estimated cross-bandpasses are of high quality, safe for a few outliers, the solutions of the individual scans still differ in quality. We came to the conclusion that scan number 143 yields a solution that can serve as a reference for a good example. The scan refers to an observation of the source 4C 39.25 at 16:24 UTC and includes data from all stations. The position of this scan is marked by the vertical dashed line in Figs 2 and 4, and we will refer to this scan as the *reference scan* in the remainder of the text.

5.1 Frequency-dependency

Figure 5 shows the cross-polarization bandpasses, determined by analyzing reference scan 143 with `PolConvert`. This serves as an example of how cross-bandpasses typically look like. The figure shows, from top to bottom, the solutions in terms of amplitude (purple) and phase (green) plotted against frequency for all stations participating in this experiment.

For all stations, amplitude and phase are not constant over the full bandwidth but are subject to considerable variability as a function of frequency. In the following, we select Onsala West as an example station to analyze the frequency-dependency of the phases in more detail and in a quantitative way. The top panel of Fig. 6 shows the cross-gain phases for station Onsala West plotted against frequency for the full observed bandwidth. It is obvious that to first order the phases follow a linear trend with frequency. The physical interpretation of this is that there is a group delay between the two linear feeds of the antenna. We fit the phase φ as a function of the frequency ν of the form

$$\varphi(\nu) = \text{fmod}(360\nu\tau + \varphi_0, 360) - 180^\circ, \quad (2)$$

where τ is the group delay and φ_0 is the phase offset. The function `fmod(x, y)` returns the floating-point remainder of the division x/y , as implemented in the `Python` `math` package. We use the `Python` `iminuit` package to fit this function to the data. The result is

$$\tau = 230 \pm 0.2 \text{ ps}, \quad (3)$$

$$\varphi_0 = -14.1^\circ \pm 0.4^\circ, \quad (4)$$

and is plotted as the solid line in the upper panel of Fig. 6. This result means that there is an overall time delay between the two linear receivers, with the signal from the V polarization arriving about 230 ps later than the signal from the H polarization. We will come back to this fit and its evolution with time in the next section.

5.2 Time-evolution

The time-evolution of the cross-bandpass phases can be seen in Fig. 7 for stations Mg, Oe, and Ow, and in Fig. 8 for stations Wf, Ws, and Yj. Each panel corresponds to one VGOS band for one station, as indicated in the plot headings. The cross-bandpass phases are expressed in color and are plotted against time in the horizontal direction and against frequency in the vertical direction. The color bar is chosen such that -180° is red, -90° is green, 0° is blue, 90° is yellow, and $+180^\circ$ is red again, in order to account for the 360° phase ambiguities. In this manner, the evolution of the cross-bandpasses can be traced over the duration of the session. In general, the cross-bandpasses remain fairly stable and

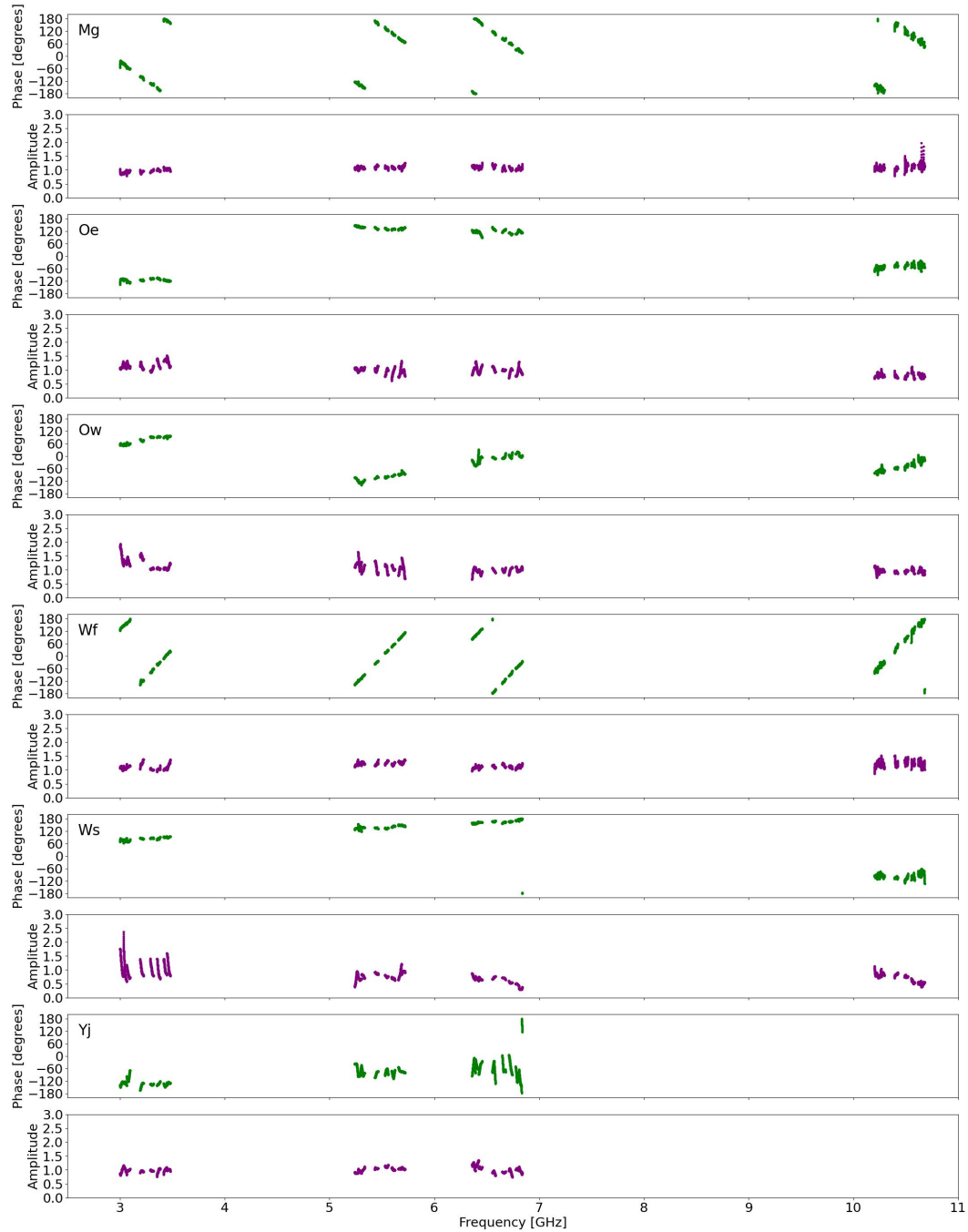


Figure 5. Cross-polarization bandpass of all stations, see Sect. 5.1 for details, resulting from analyzing scan 143 (the reference scan). For each station as labeled in the upper-left corner there is a pair of two panels: the upper panel shows the phases (green points), and the bottom one shows amplitude (purple points). Both amplitude and phase are plotted against frequency.

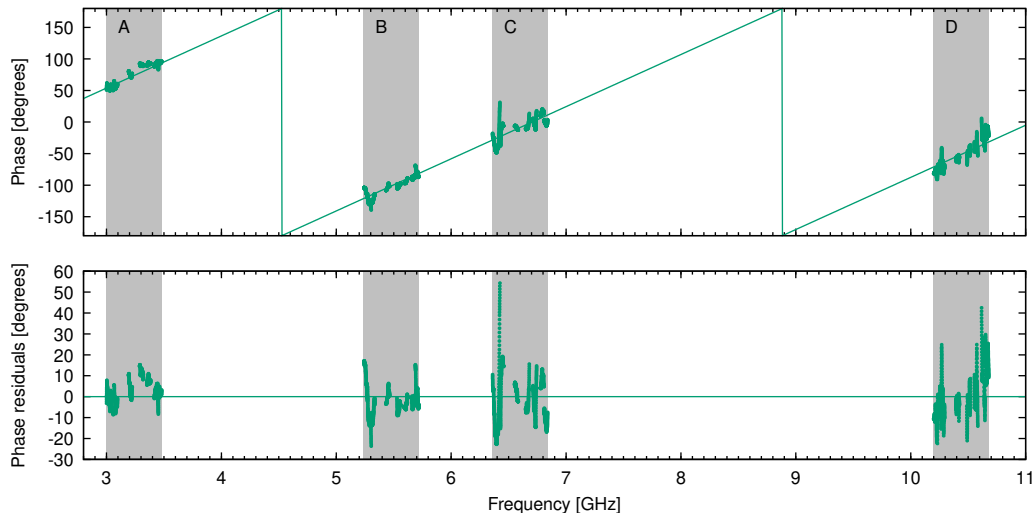


Figure 6. Top: Cross-polarization bandpass of the VGOS antenna Onsala West over the full frequency range. The solid line is a functional fit to the data. Bottom: Residuals, i.e., measured phases minus model phases. Grey-shaded areas highlight the frequency ranges of the VGOS bands, as indicated by the labels.

366 any variability evolves smoothly. There is, however, one feature that disrupts this conti-
 367 nuity, and these are three vertical stripes of sudden phase-jumps, occurring approxi-
 368 mately at times 14:00, 14:45, and 15:15 UTC. All stations are affected by this phenomenon,
 369 except for Mg, where these stripes might just not be visible because of the sparsity of
 370 the observations past 14:00. The three stripes are most pronounced in bands A and C,
 371 but there are weaker features of this type at other bands too (e.g., in band D for Oe and
 372 Ow). Another remarkable characteristic of these features is that they seem to correspond
 373 to a sudden phase offset that remains rather stable in each of these three stripes, and
 374 seems to be the same for all three stripes in each band (meaning that the three stripes
 375 within each panel have the same color, but the colors in between panels differ). We tried
 376 to investigate the origin of these three stripes, but did not come to any definite conclu-
 377 sion. The first stripe coincides with missing data from station Wf at that time, and the
 378 second stripe with missing data from Yj for VGOS band A (cf. Fig. 4). However, a solid
 379 causal relationship between the drop-out of a station and the occurrence of a stripe can-
 380 not be established, because there is not any such drop-out for the third stripe. During
 381 that time data from Mg are missing, but lack of data from that station does not lead to
 382 the appearance of any more stripes later on. For the remainder of our analysis, we treat
 383 the data from these stripes as outliers. The fact that such systematic corruption occurs
 384 is a matter of concern and the reasons should be clarification in a thorough future in-
 385 vestigation.

386 Besides the three stripes, there is clearly a certain degree of variability of the cross-
 387 bandpasses. Evident examples of this are band C of both Onsala antennas and band D
 388 of the stations Westford and Wetzell. One possible reason for these smooth variability
 389 patterns is a variability in the phase-cal signal. This could be the case, because `PolConvert`
 390 takes as a first estimate of the cross-polarization phases the differences of the phases of
 391 the phase-cal signal. For this reason, we generated plots similar to Figs 7 and 8 but for
 392 the difference of the phases of the phase-cal signals. These plots are shown in Figs 9 and 10.
 393 There is indeed a certain similarity between the variability patterns of the phase-cal phases
 394 in band C of the two Onsala and the variability patterns of the cross-bandpasses. How-
 395 ever, most of the time the phase-cal shows less variability than the cross-bandpasses. This

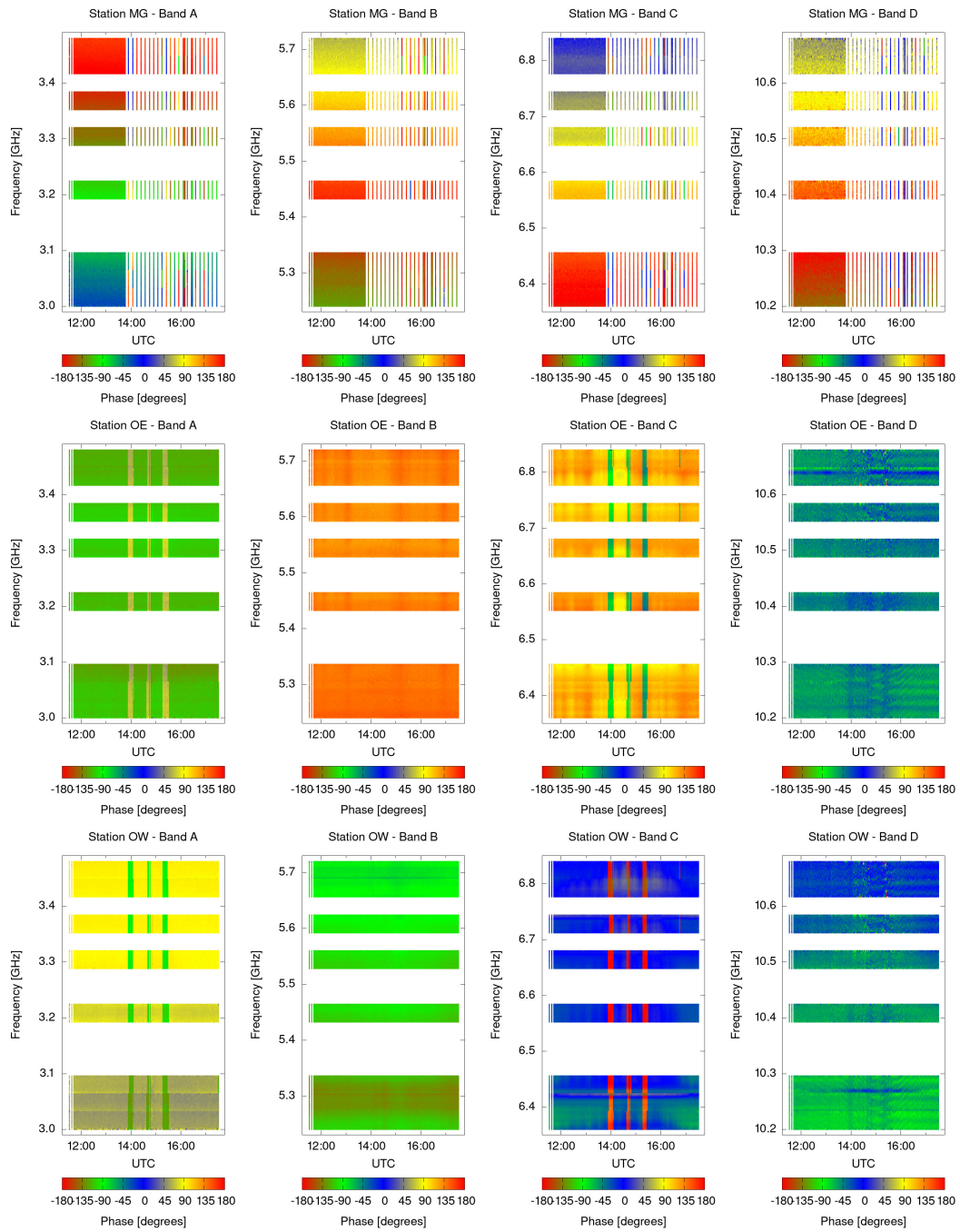


Figure 7. Time-evolution of the cross-bandpass phases, as color-coded, for stations Mg, Oe, and Ow.

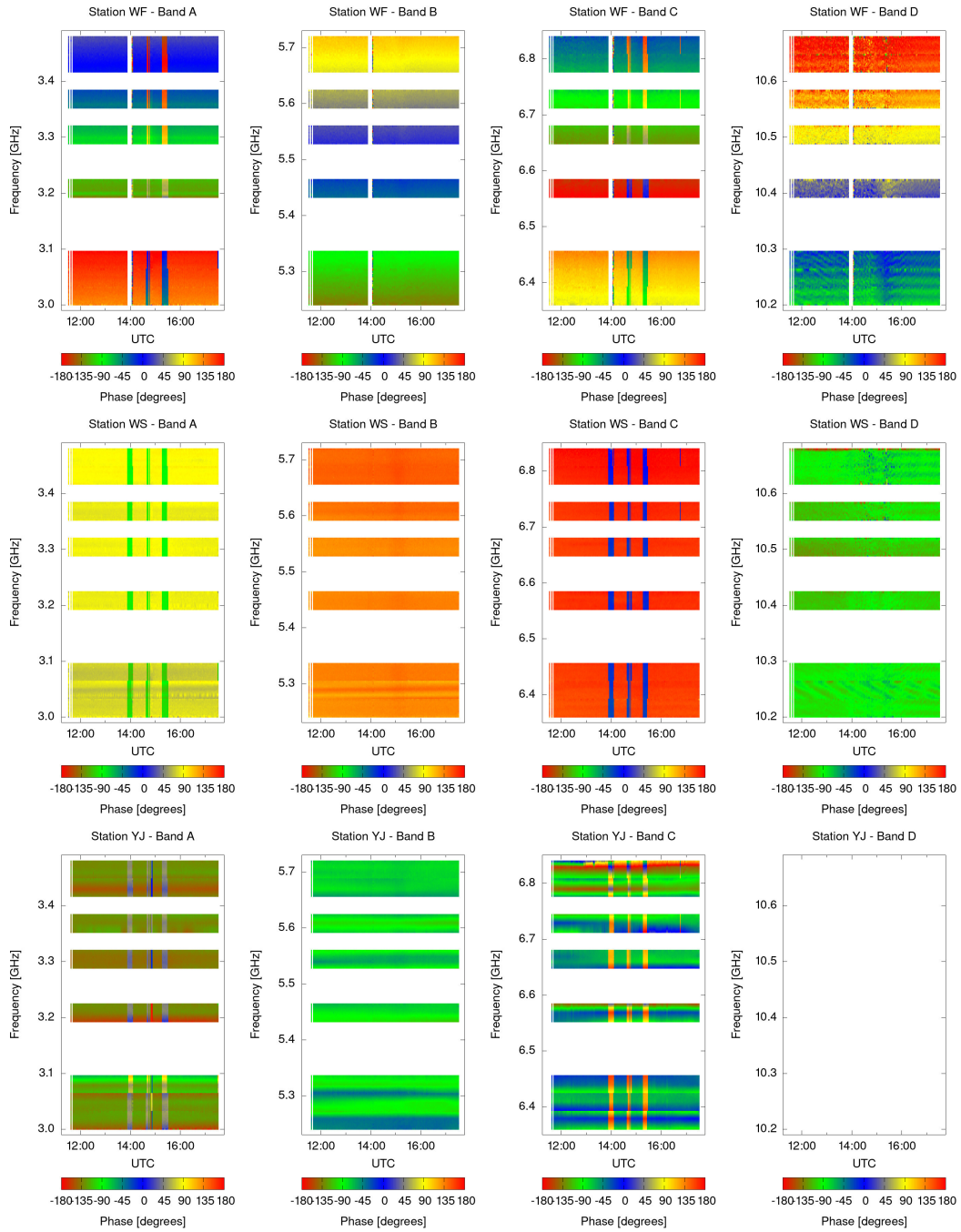


Figure 8. Same as Fig. 7 but for stations Wf, Ws, and Yj.

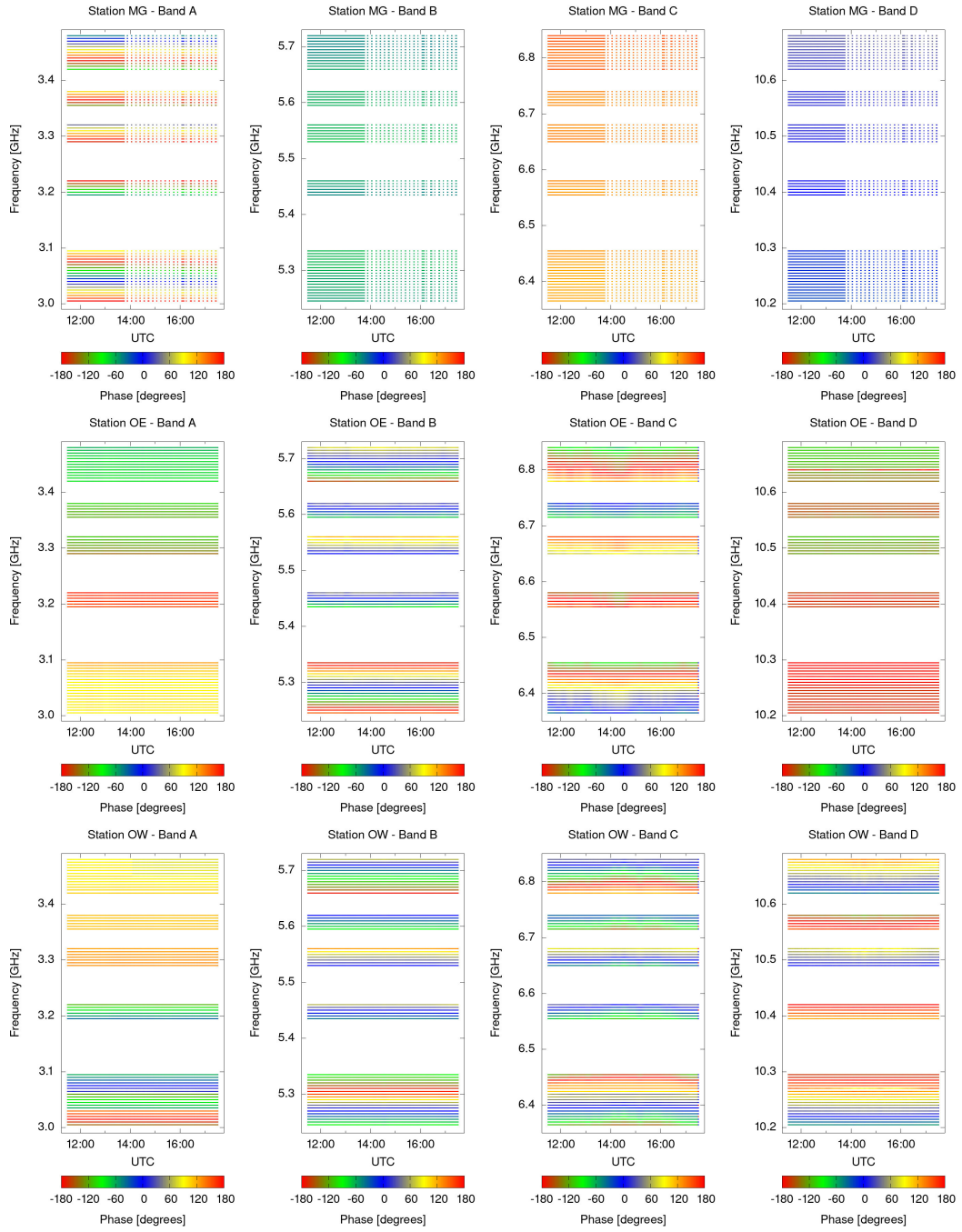


Figure 9. Time-evolution of the differential (H-V) phase-cal phases for stations Mg, Oe, and Ow.

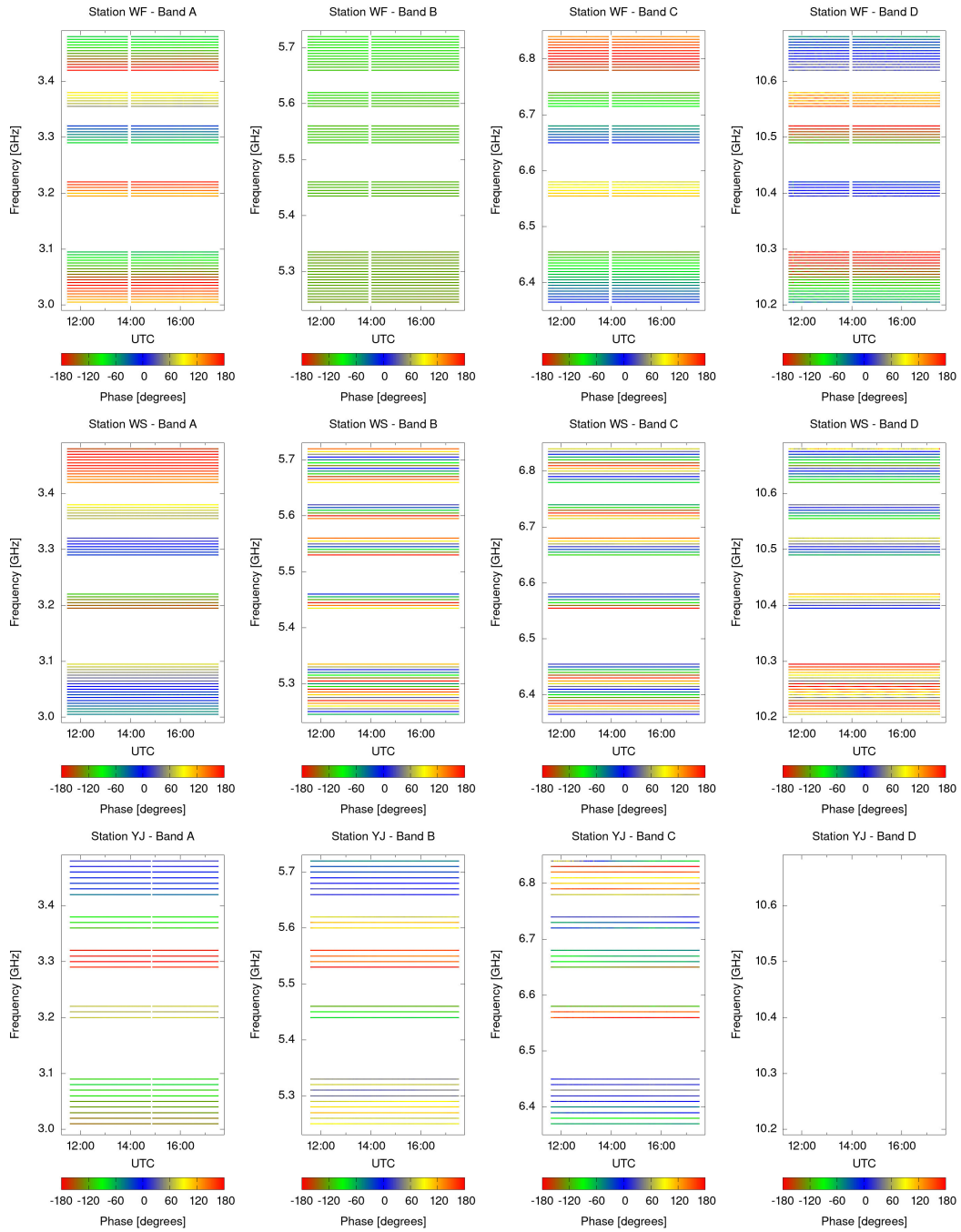


Figure 10. Same as Fig. 9 but for station Wf, Ws, and Yj.

396 is an indication that the cross-bandpasses themselves are indeed subject to some degree
397 of variability with time.

398 We have carried out the same analysis for the cross-bandpass amplitudes, and the
399 results are shown in Figs 11 and 12. There is not such a strong time-dependence of the
400 amplitude ratios, compared to the phases. What becomes evident from these plots is a
401 strong frequency dependency, which remains stable, to a certain degree, over the six hours
402 of the experiment. That there can be considerable variability in time nevertheless shows
403 the example of Yj, in the bottom row of Fig. 12, at least in some of the sub-bands. Also
404 Wf, in the top row, shows rather sudden peaks in amplitude, some of which might be
405 related to the three stripes that we saw in the phases.

406 Now we come back to station Ow and the time-evolution of the fit parameters of
407 Eq. (2) and Fig. 6, where we noticed that the phase-frequency relationship is to first order
408 characterized by a linear trend, i.e., a group delay between the two linear polariz-
409 ers within the same antenna. Here we repeat the fit of the function in Eq. (2) and ap-
410 ply it to the entire data set to obtain a time series of the parameters τ and φ_0 . We are
411 applying this fit to the data of station Onsala West, which still serves as our example
412 station. The result is plotted in Fig. 13, where panels (a) and (b) show the time series
413 of the group delay τ and the phase-offset φ_0 , respectively. There is a high degree of cor-
414 relation between these two parameters, which is in agreement with expectations because
415 a change in the slope of a line inevitably changes the position of the intersection with
416 the y -axis. In both plots (a) and (b) some outliers are clearly visible, and we highlighted
417 them in red color. These outliers were identified by an eye-examination of the data, re-
418 sulting in all data with $\tau > 240$ ps being rejected. The time of occurrence of these out-
419 liers coincides with the times of apparent disturbance, visible as the three vertical lines
420 in the plots shown in Figs 7 and 8. We identify these outliers as the result of some cor-
421 ruption in our analysis and we will not include them in any further analysis. The black
422 points in Fig. 13 (a) remain otherwise fairly stable with an average value of $\langle \tau \rangle = 230$ ps.
423 However, already on this scale, a slight trend is also visible. The phase-offset in panel (b)
424 shows a very similar picture. In order to investigate the variability of the group delay
425 in more detail, we subtract the average value $\langle \tau \rangle$ from these data. The result is shown
426 in Fig. 13 (c). One can clearly see that there is variability of the group delay in the range
427 of approximately -3 to $+3$ ps around the average value. This variability is not purely
428 random, but there are clearly systematic trends visible. There seems to be a quasi-sinusoidal
429 signal at the beginning of the time series until about 14:00 UTC, with the values oscil-
430 lating around an otherwise stable mean. The period of this oscillation seems to be about
431 half an hour. After that, the data seem to be dominated by an upward linear trend. Since
432 these data are the result of tracking one single source, antenna elevation is a relatively
433 simple function of time. This means the relationship between cross-polarization delay
434 and time could as well be dependent on elevation. In this case, gravitational deforma-
435 tions of the instrument could play a role. It also is worth mentioning that the change
436 in behavior at around 14:00 UTC coincides with the first occurrence of the disturbance,
437 i.e., the first of the three vertical lines in Figs 7 and 8.

438 5.3 Results for sources NRAO 150 and OJ 287

439 At the beginning of the session er2201, we included two 5-min scans to two other
440 sources. These sources were NRAO 150 and OJ 287, which we identified as potential cross-
441 bandpass calibrators based on our experience from past experiments. We find that re-
442 sults obtained from observations of 4C 39.25 are still superior to those obtained from ob-
443 servations of these two other sources. This is visualized in Fig. 14, where we show the
444 phases of the cross-gain solutions for band A, sub-band 5, for the station Onsala West.
445 Panel (a) shows the results for NRAO 150, (b) for OJ 287, and (c) for 4C 39.25. All three
446 results were obtained from analyzing 2-minute scans, cut from the original 5-minute scans
447 for NRAO 150 and OJ 287, and from the first 10-minute scan of 4C 39.25. We turned

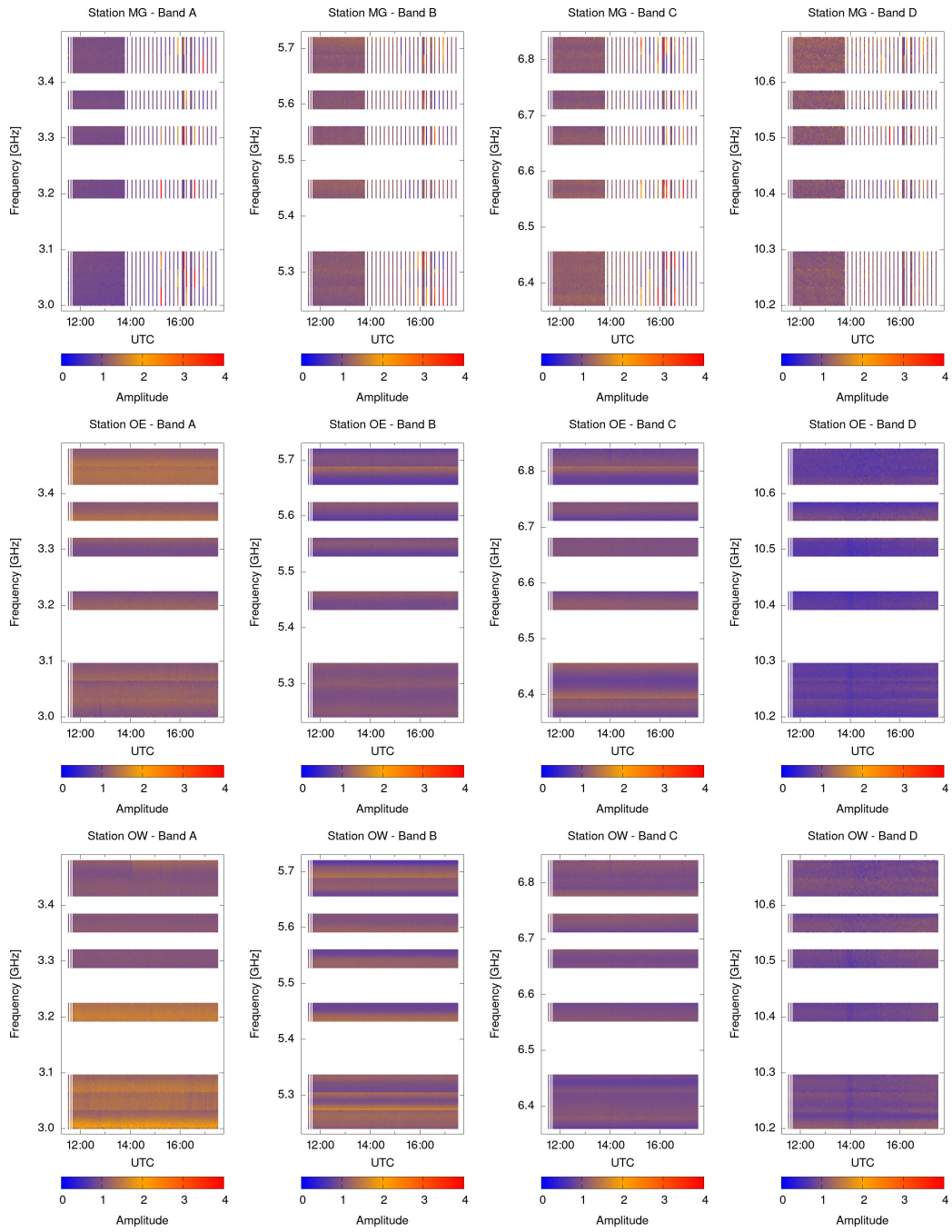


Figure 11. Time-evolution of the cross-bandpass amplitudes, as color-coded, for stations Mg, Oe, and Ow.

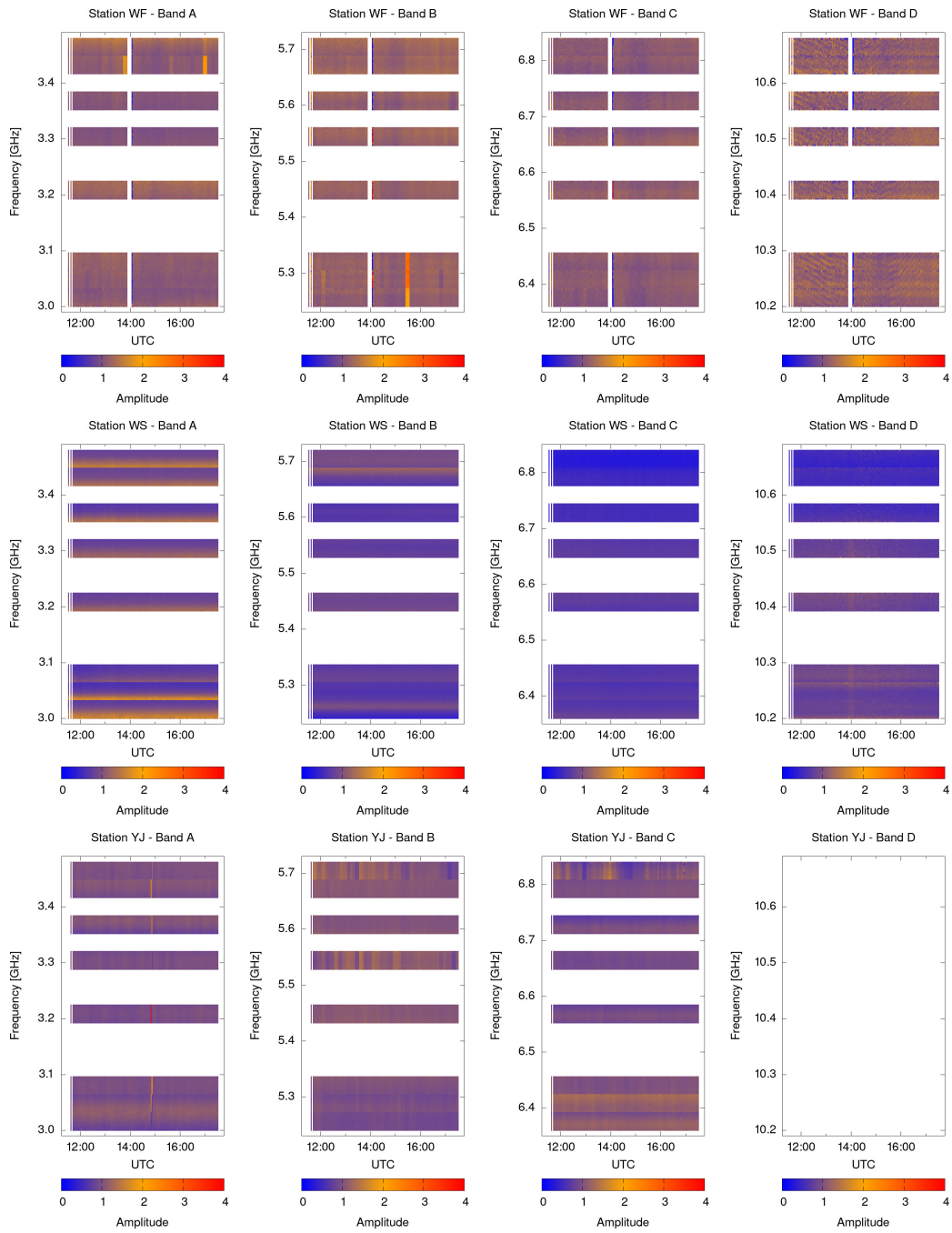


Figure 12. Same as Fig. 11 but for stations Wf, Ws, and Yj.

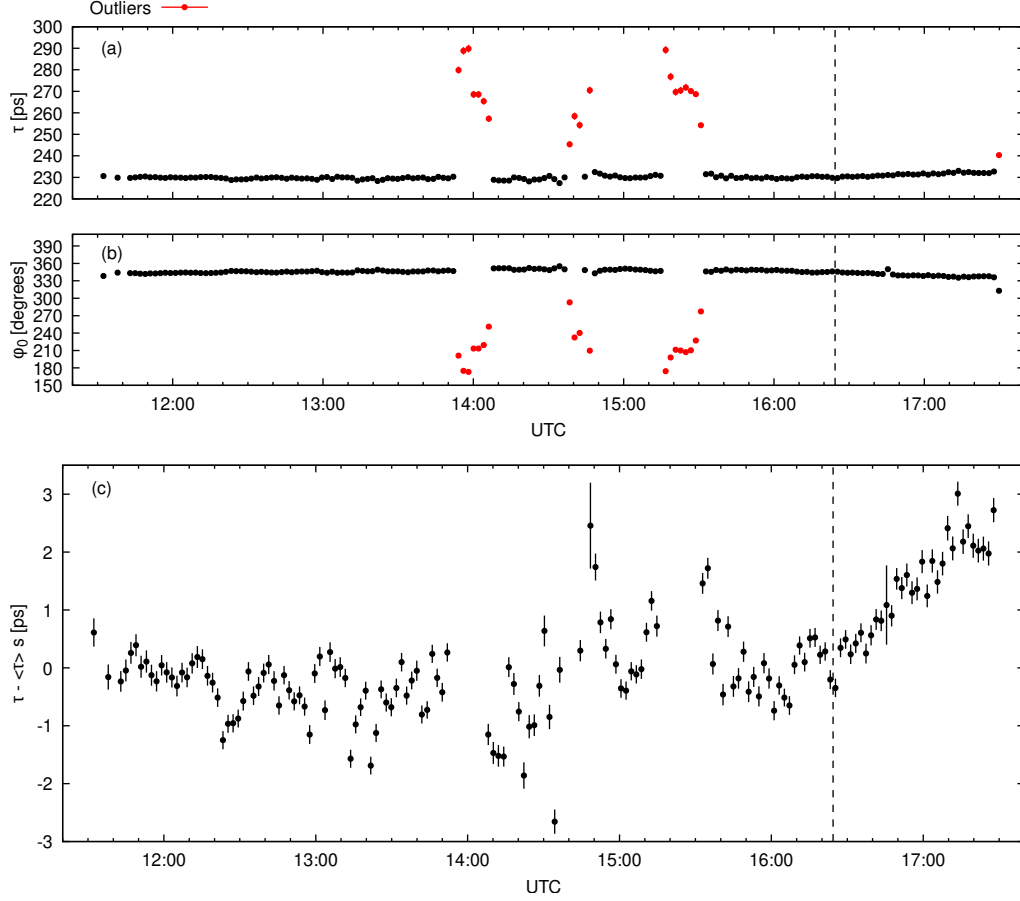


Figure 13. Time-evolution of the parameters obtained from fitting Eq. (2) to the entire data set for station Ow. Outliers appear in red color and are not used for further analysis. The position of the reference scan 143 is marked by the vertical dashed line. (a) Group delay τ between H and V polarization. (b) Phase-offset φ_0 . (c) Group delay τ with outliers removed and the average value of $\langle \tau \rangle = 230$ ps subtracted. Variability in the range ± 3 ps can be seen along with some clearly systematic trends.

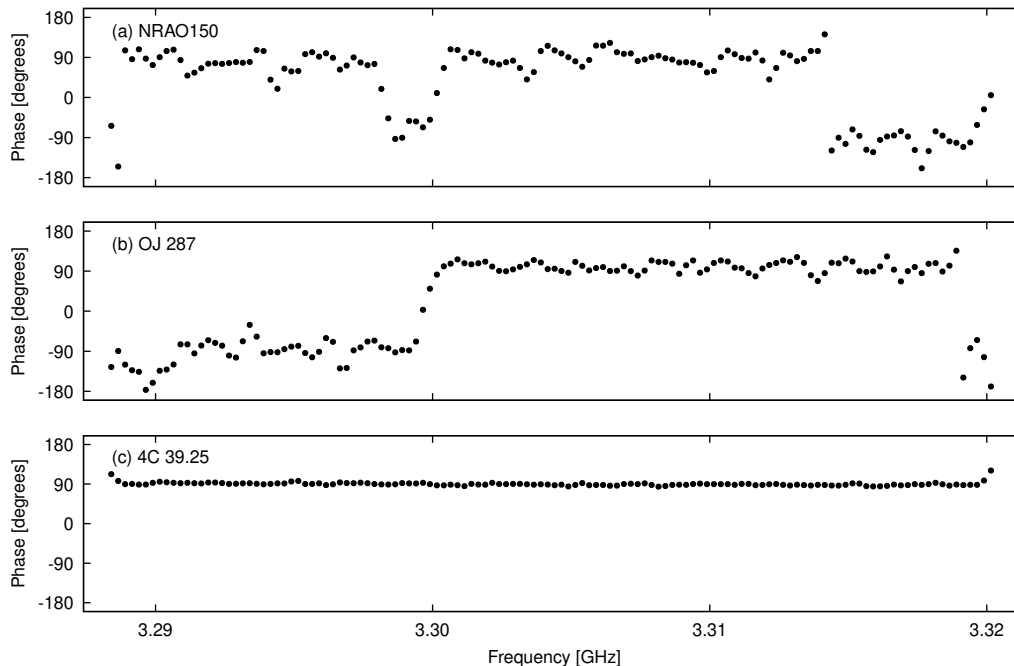


Figure 14. Cross-polarization bandpasses obtained from observations of (a) NRAO 150, (b) OJ 287, and (c) 4C 39.25. The three results were obtained from 2-min scans. The superior quality of 4C 39.25 is evident.

448 off any frequency averaging in `PolConvert` because this allows to better see the signal-
 449 to-noise ratio. Time averaging was set to 20 seconds, as for the remainder of the results
 450 shown in this article. It is obvious by eye that the solution for 4C 39.25 looks much cleaner
 451 than the solutions for the two other sources. The phases obtained from both other sources
 452 are much noisier than those obtained from 4C 39.25. In addition to the noise, there are
 453 also systematic effects visible in the two other bandpasses, which are not present in panel (c).
 454 Both panels (a) and (b) show an effect that can be described as 180° -ambiguities, which
 455 correspond to a sign flip of the complex cross-gain values. In panel (c) the phase is basi-
 456 cally stable at a value of $\sim 90^\circ$. In panels (a) and (b) the majority of the phases are
 457 scattered around 90° , but for some frequency intervals the phase is shifted to $\sim -90^\circ$,
 458 i.e., 180° downwards. In panel (a) this is visible at around 3.30 GHz and towards 3.32 GHz,
 459 and in panel (b) the phases cluster around -90° from the beginning of the sub-band until
 460 3.30 GHz and around $+90^\circ$ from that point on until the end of the sub-band. These
 461 systematic offsets are not present at all in the solution obtained from 4C 39.25.

462 The results shown in Fig. 14 and described here serve as an example to illustrate
 463 the superior quality of 4C 39.25 compared to other potential cross-bandpass calibrators,
 464 that have been investigated so far. They are representative of the results that we have
 465 obtained at other frequency ranges in this experiment and also in other experiments car-
 466 ried out in the past.

467 The suitability of 4C 39.25 as a calibrator might be surprising given the fact that
 468 it shows an extended VLBI morphology at cm wavelengths (as already pointed out in
 469 Sect. 2). The extended structure of this source is also mentioned in the context of the
 470 third realization of the international celestial reference frame (ICRF3) (Charlot et al.,
 471 2020). In ICRF2 (Fey et al., 2015) it was even treated as a “special handling source”,
 472 as a consequence of its temporal source position variability, showing that its radio mor-

Table 4. Cross-polarization delay estimates derived from observations of 4C 39.25 in different sessions. Concerning the delay uncertainties, for the first three sessions these are the nominal uncertainties from the least squares fit to a single scan, for session er2201 this is the range of values that we see in Fig. 13.

Date (MM/DD/YYYY)	Session name	Delay [ps]
07/08/2019	ev9189	223.5 ± 0.3
07/22/2019	ev9203	224.3 ± 0.3
08/08/2019	ev9217	228.4 ± 0.4
09/08/2022	er2201	230 ± 3

473 phology is even subject to considerable changes over time. The concept of special handling
 474 source was abandoned in ICRF3. In the discussion of these issues it is important
 475 to point out that the quantities which are estimated by PolConvert in the analysis pre-
 476 sented in this article, i.e., the cross-polarization gains, are not affected by source struc-
 477 ture, as long as the structure is not polarized. Only the polarized part of the radio source
 478 structure would affect the estimation of the cross-polarization gains.

479 5.4 Long-term cross-bandpass stability

480 One of the aims of experiment er2201 was to investigate the time-evolution of VGOS
 481 cross-bandpasses over the duration of six hours. Here we discuss the long-term stabil-
 482 ity of cross-bandpasses over time scales of years. For this purpose, we make use of ob-
 483 servations of 4C 39.25 in previous EU-VGOS (Albentosa et al., 2023, and references therein)
 484 sessions. The source was observed in the following sessions: ev9189, ev9203, ev9217.

485 Figure 15 shows the cross-bandpass solutions for Onsala West from observations
 486 of 4C 39.25 in sessions ev9189 (top panel, observed on July 8 2019), ev9203 (middle panel,
 487 July 22 2019), and ev9217 (bottom panel, August 5 2019). First of all, in all three pan-
 488 els, the value of the overall group delay is similar, within a range of a few picoseconds.
 489 The exact estimates of the cross-polarization delays are listed in Table 4, where we also
 490 include a value for the session er2201. There is, however, an important difference between
 491 the first three and the last delay value in this table. While the first three values are de-
 492 rived from single scans, the value for er2201 is the average value (230 ps) of all delays
 493 plotted in Fig. 13 (a), excluding the outliers. Because, as evident from Fig. 13 (c), the
 494 scatter of the delays is not dominated by Gaussian noise but rather shows clear system-
 495 atics, we do not report the uncertainty of the mean value (which is 1 ps) but instead the
 496 range of values that we see in this figure, i.e., ± 3 ps. The similarity of all four values is
 497 an indication that the delay between the two polarizers within one antenna can remain
 498 remarkably stable, even over a time span of several years, to within a few picoseconds.

499 However, there is also a component of the cross-polarization bandpasses that is con-
 500 siderably variable over time-scales of years, and these are the residuals after subtract-
 501 ing the group delay. These residuals are shown in the lower panels in Fig. 15. These vari-
 502 ations are sometimes larger than the intrinsic scatter of the data points, as visible for
 503 example in the uppermost residual plot in the figure (referring to ev9189). This is an in-
 504 dication that these variations can be significant.

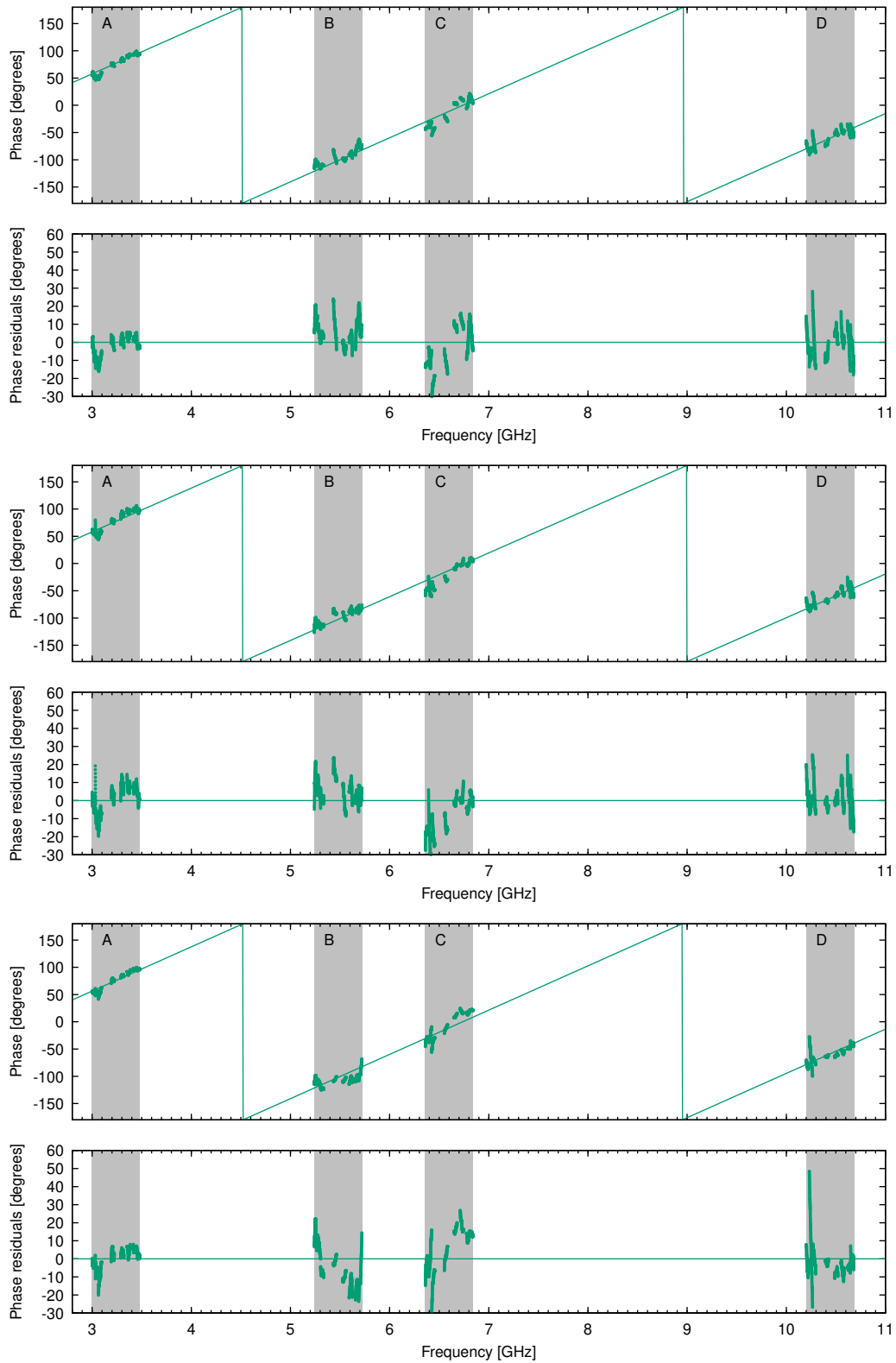


Figure 15. Cross-bandpass solutions for Onsala West from observations of 4C 39.25 in other EU-VGOS sessions. Top: ev9189, scan 115. Middle: ev9203, scan 115. Bottom: ev9217, scan 115.

6 Conclusions

In this article, we presented the results from a six-hour VLBI (VGOS) session consisting of cross-polarization bandpass calibrator scans of the source 4C 39.25. These are our conclusions:

1. The radio-loud AGN 4C 39.25 is confirmed as an excellent calibrator for the measurement of cross-polarization bandpasses of linearly polarized radio telescopes. Observations of this source still lead to the cleanest measurements that we have seen so far, compared to other sources (e.g., Fig. 14). This statement is based on observations between 3 and 11 GHz. The suitability as a calibrator at other frequencies (e.g., mm wavelengths) should be subject of a future investigation.
2. We measured the cross-bandpasses for the VGOS antennas Mg, Oe, Ow, Wf, Ws, and Yj. The phases are to first order characterized by a group delay in the ~ 100 ps regime, which remains stable over the six hours of the experiment with a variability of a few picoseconds. In our example, the remaining temporal variability of this delay is clearly characterized by systematic trends like oscillations and linear drifts (Fig. 13 c).
3. After removing a linear trend (i.e., group delay) from the cross-polarization phases, there is still considerable scatter as a function of frequency. In the time-domain, these phase-residuals show systematic and smooth transitions over the course of six hours of the experiment (cf. Figs 7 and 8).
4. Investigation of the long-term evolution of the cross-polarization delays shows that the delay can remain stable, but that the phase-scatter on top of the delay is still significantly variable (see Fig. 15 and Table 4).
5. The cross-bandpass amplitudes are not constant over sub-bands, but show distinct shapes in frequency. This frequency-dependency has to be taken into account in cross-bandpass calibration.

The results obtained in our investigation can be useful for the adjustment of calibration strategies of VGOS sessions and other VLBI experiments including stations observing with linear feeds. These results show that cross-polarization bandpasses change systematically with time. This means that taking the average, e.g., over one VGOS session is, strictly speaking, not valid. The underlying systemics can be removed from the data by applying a time-dependent calibration. We recommend including dedicated calibration scans in VGOS schedules. Two-minute scans of 4C 39.25 can be used for an improved calibration of VGOS data, which has in turn the potential of increasing the signal-to-noise ratio of databases and geodetic and astrometric results. It might be beneficial to update the cross-bandpasses multiple times per session, with a cadence of once per hour. In any case, it is highly recommended to include multiple calibrator scans for the sake of redundancy, because as we have seen here, calibration can at times be subject to corruption (see the three stripes in Figs 7 and 8). The exact impact, which the systematic cross-bandpass variability and its correction may have on the subsequent analysis should be the subject of a future investigation. Concerning the magnitude of the corrections, geophysical models and interpretations have improved down to the millimetre over the last decade. This is discussed, e.g., in the context of the latest realization of the International Terrestrial Reference Frame (ITRF2020) (Altamimi et al., 2023, and references therein). This means that the quality of the observations needs to be maintained at the same level, i.e., ~ 3 ps., which matches the magnitude of the systematic variability of the cross-polarization delay reported here.

Calibrator scans are optimized for the purpose of estimating parameters that are intrinsic to the instrument, this article focusing on the example of cross-polarization gains. In this respect, calibrator scans are useful for removing systematic errors from the data and also increase the signal-to-noise ratio. As a consequence, calibration has the positive effect of improving the accuracy of parameters of interest, estimated during the ana-

557 lysis of the session. Calibrator scans are, however, not necessarily optimized to be di-
 558 rectly useful, by themselves, for the estimation of these parameters. The following elab-
 559 orates on potential deteriorating effects which the inclusion of calibration scans might
 560 have on the analysis of the session. The inclusion of calibrator scans into geodetic/astrometric
 561 VLBI sessions comes at the prize of reducing the observing time spent on scans that are
 562 optimized for the actual purpose of the experiment. One important aspect in this con-
 563 text is sky-coverage, which is crucial for the estimation of tropospheric parameters. VGOS
 564 sessions including one two-minute calibrator scan per hour have already been observed,
 565 and the effect of scan loss due to additional calibrator scans is marginal. Current VGOS
 566 schedules contain about 100 scans per hour, i.e., approximately one scan every 36 sec-
 567 onds. Including one 120-seconds scan per hour would potentially mean a loss of three
 568 regular scans per hour, i.e., three per cent of all scans of the session. This loss is not sig-
 569 nificant for the following reasons. In practice, current VGOS sessions are subject to tech-
 570 nical problems that cause a scan loss rate that is already significantly higher than three
 571 per cent. This scan loss has not resulted in any significant degradation of the tropospheric
 572 estimation. In any case, a carefully prepared schedule will include the calibration scans
 573 in such a way that the degradation of sky-coverage will be kept to a minimum. The cur-
 574 rent 100 scans per hour leave a lot of headroom for the present parametrization of the
 575 analysis of VGOS sessions, also for the estimation of the other parameters of interest.
 576 In summary, in a carefully prepared schedule, the positive effects of the calibration will
 577 outweigh the marginal effects of scan loss.

578 The question of what it is that makes 4C 39.25 such an outstanding calibrator for
 579 the purpose of the measurement of linear cross-polarization bandpasses will be subject
 580 of a future investigation. Certainly, 4C 39.25 is one of the brightest AGN in the radio
 581 sky. However, we have the strong impression that brightness is not the only character-
 582 istic that sets this source apart, because observations of similarly bright sources have,
 583 so far, not given any similarly good results. The analysis of a dedicated survey of a large
 584 number of candidate sources will help to answer this question and increase the number
 585 of useful calibrators. An investigation of this nature is currently in progress and will be
 586 presented in a future publication.

587 Acronyms

588 **AGN** Active Galactic Nucleus
 589 **ALMA** Atacama Large Millimeter/submillimeter Array
 590 **HOPS** Haystack Observatory Postprocessing System
 591 **IONEX** IONospheric map EXchange
 592 **MOJAVE** Monitoring Of Jets in Active galactic nuclei with VLBA Experiments
 593 **MIT** Masseurhusetts Institute of Technology
 594 **R&D** Research and Development
 595 **SNR** Signal-to-noise ratio
 596 **TEC** Total electron content
 597 **VLBA** Very Long Baseline Array
 598 **VLBI** Very Long Baseline Interferometry
 599 **VGOS** VLBI Global Observing System
 600 **VSC** Vienna Scientific Cluster

601 Open Research Section

602 The VLBI Level-1A correlator output data for the experiment er2201 can be ob-
 603 tained from NASA's crustal dynamics data information system (CDDIS, Noll, 2010) at
 604 [https://cddis.nasa.gov/archive/vlbi/ivsdata/swin/2022/20220908.er2201_v001](https://cddis.nasa.gov/archive/vlbi/ivsdata/swin/2022/20220908.er2201_v001_swin.tar.bz2)
 605 [_swin.tar.bz2](https://cddis.nasa.gov/archive/vlbi/ivsdata/swin/2022/20220908.er2201_v001_swin.tar.bz2) (CDDIS, 2023). Registration is necessary. If you use these data for pub-

606 lication, please acknowledge the CDDIS and the IVS (Nothnagel et al., 2017). DiFX is
 607 available at <https://www.atnf.csiro.au/vlbi/dokuwiki/doku.php/difx/installation>
 608 along with installation instructions. PolConvert is available from github: [https://github](https://github.com/marti-vidal-i/PolConvert)
 609 [.com/marti-vidal-i/PolConvert](https://github.com/marti-vidal-i/PolConvert). Will be uploaded to a repository if accepted.

610 Acknowledgments

611 We thank Sergio Dzib from the MPIfR for carefully reading the manuscript, and Inmac-
 612 ulada Malo-Gómez from Yebes Observatory for useful discussions about hybrid couplers.
 613 This research made use of data obtained from observations carried out by the Interna-
 614 tional VLBI Service (Nothnagel et al., 2017). The computational results presented have
 615 been achieved in part using the Vienna Scientific Cluster (VSC). This research was funded
 616 in whole, or in part, by the Austrian Science Fund (FWF) [P 35920]. For the purpose
 617 of open access, the author has applied a CC BY public copyright licence to any Author
 618 Accepted Manuscript version arising from this submission.

619 References

- 620 Abdalmalak, K. A., Santamaría-Botello, G., Llorente-Romano, S., Rivera-Lavado,
 621 A., Flygare, J., Lopez Fernandez, J., ... Garcia-Munoz, L. (2020, 03). Ul-
 622 trawideband conical log-spiral circularly polarized feed for radio astronomy.
 623 *IEEE Transactions on Antennas and Propagation*, 68, 1995 - 2007. doi:
 624 10.1109/TAP.2019.2949700
- 625 Albertosa, E., Alef, W., Bernhart, S., Böhm, J., Bolaño González, R., Choi, Y. K.,
 626 ... Verkouter, M. (2023, January). Current Status of the EU-VGOS Project.
 627 In K. L. Armstrong, D. Behrend, & K. D. Baver (Eds.), *International vlbi ser-*
 628 *vice for geodesy and astrometry 2022 general meeting proceedings* (p. 85-89).
- 629 Alberdi, A., Gómez, J. L., Marcaide, J. M., Marscher, A. P., & Pérez-Torres, M. A.
 630 (2000, September). 4C 39.25: Witnessing the interaction between a moving
 631 and a stationary component. *Astronomy & Astrophysics*, 361, 529-534.
- 632 Alef, W., Anderson, J. M., Bernhart, S., de Vicente, P., González García, J., Haas,
 633 R., ... Wagner, J. (2019a, November). The European-VGOS Project. In
 634 R. Haas, S. Garcia-Espada, & J. A. López Fernández (Eds.), *Proceedings of the*
 635 *24th european vlbi group for geodesy and astrometry working meeting* (Vol. 24,
 636 p. 107-111).
- 637 Alef, W., Anderson, J. M., Bernhart, S., de Vicente, P., González García, J., Haas,
 638 R., ... Wagner, J. (2019b, November). The European-VGOS Project. In
 639 R. Haas, S. Garcia-Espada, & J. A. López Fernández (Eds.), *Proceedings of the*
 640 *24th european vlbi group for geodesy and astrometry working meeting* (Vol. 24,
 641 p. 107-111).
- 642 Alef, W., Tuccari, G., Dornbusch, S., Roy, A. L., Wunderlich, M., Kasemann, C., ...
 643 Bezrukovs, V. (2019, November). BRAND - A Wideband Receiver for Astron-
 644 omy and Geodesy. In R. Haas, S. Garcia-Espada, & J. A. López Fernández
 645 (Eds.), *Proceedings of the 24th european vlbi group for geodesy and astrometry*
 646 *working meeting* (Vol. 24, p. 31-36).
- 647 Aller, H. D. (1970, July). The Polarization of Variable Radio Sources at 8 GHz. I.
 648 The Observations. *The Astrophysical Journal*, 161, 1. doi: 10.1086/150508
- 649 Altamimi, Z., Rebischung, P., Collilieux, X., Métivier, L., & Chanard, K. (2023,
 650 May). ITRF2020: an augmented reference frame refining the model-
 651 ing of nonlinear station motions. *Journal of Geodesy*, 97(5), 47. doi:
 652 10.1007/s00190-023-01738-w
- 653 Berge, G. L., & Seielstad, G. A. (1969, July). Polarisation Measurements of Extra-
 654 galactic Radio Sources at 3.12-CM Wave-Length. *The Astrophysical Journal*,
 655 157, 35. doi: 10.1086/150047
- 656 Bignell, R. C., & Seaquist, E. R. (1973, September). Observations of the linear po-

- 657 larization of radio sources at 2.8 and 4.5 CM. *The Astronomical Journal*, 78,
658 536. doi: 10.1086/111454
- 659 CDDIS. (2023). *International vlbi service for geodesy and astrometry (ivs) vlbi level*
660 *1a correlator output [online]. available from the nasa crustal dynamics data*
661 *information system daac, greenbelt, md, usa. accessed october 18, 2023.* doi:
662 10.5067/VLBI/vlbi_11a_swin_001
- 663 Charlot, P., Jacobs, C. S., Gordon, D., Lambert, S., de Witt, A., Böhm, J., ...
664 Gaume, R. (2020, December). The third realization of the International Ce-
665 lestial Reference Frame by very long baseline interferometry. *Astronomy &*
666 *Astrophysics*, 644, A159. doi: 10.1051/0004-6361/202038368
- 667 Deller, A. T., Brisken, W. F., Phillips, C. J., Morgan, J., Alef, W., Cappallo, R., ...
668 Wayth, R. (2011, March). DiFX-2: A More Flexible, Efficient, Robust, and
669 Powerful Software Correlator. *Publications of the Astronomical Society of the*
670 *Pacific*, 123(901), 275. doi: 10.1086/658907
- 671 Event Horizon Telescope Collaboration, Akiyama, K., Alberdi, A., Alef, W., Asada,
672 K., Azulay, R., ... Ziurys, L. (2019, April). First M87 Event Horizon Tele-
673 scope Results. I. The Shadow of the Supermassive Black Hole. *The Astrophysic-*
674 *ical Journal*, 875(1), L1. doi: 10.3847/2041-8213/ab0ec7
- 675 Fey, A. L., Gordon, D., Jacobs, C. S., Ma, C., Gaume, R. A., Arias, E. F., ...
676 Zharov, V. (2015, August). The Second Realization of the International Cele-
677 stial Reference Frame by Very Long Baseline Interferometry. *The Astronomical*
678 *Journal*, 150(2), 58. doi: 10.1088/0004-6256/150/2/58
- 679 García-Pérez, O., Terceroc, F., Malo, I., Gallego, J. D., & López-Pérez, J. A. (2018).
680 *Linear to circular polarization conversion using microwave hybrids for BRAND*
681 *(1.5-15.5 GHz)* (CDT Technical Report No. 2018-12). Observatorio de Yebes
682 Guadalajara (Spain).
- 683 García-Pérez, O., Terceroc, F., Malo, I., & López-Pérez, J. A. (2018). *Linear to cir-*
684 *cular polarization conversion using microwave hybrids for VGOS (2-14 GHz)*
685 (CDT Technical Report No. 2018-13). Observatorio de Yebes Guadalajara
686 (Spain).
- 687 Impey, C. D., & Tapia, S. (1990, May). The Optical Polarization Properties of
688 Quasars. *The Astrophysical Journal*, 354, 124. doi: 10.1086/168672
- 689 Jaradat, A., Jaron, F., Gruber, J., & Nothnagel, A. (2021, August). Considerations
690 of VLBI transmitters on Galileo satellites. *Advances in Space Research*, 68(3),
691 1281-1300. doi: 10.1016/j.asr.2021.04.048
- 692 Jaron, F., Bernhart, S., Böhm, J., González García, J., Gruber, J., Choi, Y. K., ...
693 EU-VGOS Collaboration (2021, December). EU-VGOS activities in Vienna.
694 In R. Haas (Ed.), *25th european vlbi group for geodesy and astrometry working*
695 *meeting* (Vol. 25, p. 19-23).
- 696 Khudchenko, A., Fominsky, M., Heiter, C., Heyminck, S., Gusten, R., Klein, B.,
697 ... Dmitriev, P. N. (2019, November). Design and Performance of a Side-
698 band Separating SIS Mixer for 800-950 GHz. *IEEE Transactions on Terahertz*
699 *Science and Technology*, 9(6), 532-539. doi: 10.1109/TTHZ.2019.2939003
- 700 Kooi, J., Soriano, M., Bowen, J., Abdulla, Z., Samoska, L., Fung, A., ... Lazio, J.
701 (2023, February). A Multioctave 8 GHz-40 GHz Receiver for Radio Astronomy.
702 *IEEE Journal of Microwaves*, 3, 570-586. doi: 10.1109/JMW.2023.3237693
- 703 López-Pérez, J. A., Tercero-Martínez, F., Serna-Puente, J. M., Vaquero-Jiménez, B.,
704 Patino-Esteban, M., García-Carreño, P., ... López-Fernández, J. A. (2021,
705 April). A Tri-Band Cooled Receiver for Geodetic VLBI. *Sensors*, 21(8), 2662.
706 doi: 10.3390/s21082662
- 707 Malo-Gomez, I., Gallego-Puyol, J. D., Diez-Gonzalez, C., Lopez-Fernandez,
708 I., & Briso-Rodriguez, C. (2009, December). Cryogenic Hybrid Cou-
709 pler for Ultra-Low-Noise Radio Astronomy Balanced Amplifiers. *IEEE*
710 *Transactions on Microwave Theory Techniques*, 57(12), 3239-3245. doi:
711 10.1109/TMTT.2009.2033874

- 712 Martí-Vidal, I., Mus, A., Janssen, M., de Vicente, P., & González, J. (2021, Febru-
713 ary). Polarization calibration techniques for the new-generation VLBI. *Astron-*
714 *omy & Astrophysics*, *646*, A52. doi: 10.1051/0004-6361/202039527
- 715 Martí-Vidal, I., Roy, A., Conway, J., & Zensus, A. J. (2016, March). Cali-
716 bration of mixed-polarization interferometric observations. Tools for the
717 reduction of interferometric data from elements with linear and circu-
718 lar polarization receivers. *Astronomy & Astrophysics*, *587*, A143. doi:
719 10.1051/0004-6361/201526063
- 720 Nartallo, R., Gear, W. K., Murray, A. G., Robson, E. I., & Hough, J. H. (1998,
721 July). A Millimetre/Submillimetre Polarization Survey of Compact Flat-
722 Spectrum Radio Sources. *Monthly Notices of the Royal Astronomical Society*,
723 *297*(3), 667-686. doi: 10.1046/j.1365-8711.1998.01405.x
- 724 Niell, A., Barrett, J., Burns, A., Cappallo, R., Corey, B., Derome, M., . . . Petra-
725 chenko, B. (2018, October). Demonstration of a Broadband Very Long
726 Baseline Interferometer System: A New Instrument for High-Precision Space
727 Geodesy. *Radio Science*, *53*(10), 1269-1291. doi: 10.1029/2018RS006617
- 728 Noll, C. E. (2010). The crustal dynamics data information system: A resource
729 to support scientific analysis using space geodesy. *Advances in Space Re-*
730 *search*, *45*(12), 1421-1440. Retrieved from [https://www.sciencedirect.com/](https://www.sciencedirect.com/science/article/pii/S0273117710000530)
731 [science/article/pii/S0273117710000530](https://www.sciencedirect.com/science/article/pii/S0273117710000530) (DORIS: Scientific Applications
732 in Geodesy and Geodynamics) doi: <https://doi.org/10.1016/j.asr.2010.01.018>
- 733 Nothnagel, A., Artz, T., Behrend, D., & Malkin, Z. (2017, July). International VLBI
734 Service for Geodesy and Astrometry. Delivering high-quality products and
735 embarking on observations of the next generation. *Journal of Geodesy*, *91*(7),
736 711-721. doi: 10.1007/s00190-016-0950-5
- 737 Petrachenko, B., Niell, A., Behrend, D., Corey, B., Boehm, J., Charlot, P., . . . Wres-
738 nik, J. (2009, June). *Design Aspects of the VLBI2010 System. Progress Report*
739 *of the IVS VLBI2010 Committee, June 2009*. NASA/TM-2009-214180, 2009,
740 62 pages.
- 741 Pilkington, J. D. H., & Scott, J. F. (1965, January). A survey of radio sources be-
742 tween declinations 20° and 40°. *Memoirs of the Royal Astronomical Society*,
743 *69*, 183.
- 744 Schartner, M., & Böhm, J. (2019, August). VieSched++: A New VLBI Scheduling
745 Software for Geodesy and Astrometry. *Publications of the Astronomical Society*
746 *of the Pacific*, *131*(1002), 084501. doi: 10.1088/1538-3873/ab1820
- 747 Sovers, O. J., Fanselow, J. L., & Jacobs, C. S. (1998, October). Astrometry and
748 geodesy with radio interferometry: experiments, models, results. *Reviews of*
749 *Modern Physics*, *70*(4), 1393-1454. doi: 10.1103/RevModPhys.70.1393
- 750 Thompson, A. R., Moran, J. M., & Swenson, J., George W. (2017). *Interferometry*
751 *and Synthesis in Radio Astronomy, 3rd Edition*. doi: 10.1007/978-3-319-44431
752 -4
- 753 Zhao, G.-Y., Gómez, J. L., Fuentes, A., Krichbaum, T. P., Traianou, E., Lico, R.,
754 . . . Toscano, T. (2022, June). Unraveling the Innermost Jet Structure of OJ
755 287 with the First GMVA + ALMA Observations. *The Astrophysical Journal*,
756 *932*(1), 72. doi: 10.3847/1538-4357/ac6b9c